Translational Oncology
www.transonc.com

Volume 10 Number 4 August 2017 pp. 555–569 555

The Expression of Connexins and SOX2 Reflects the Plasticity of Glioma Stem-Like Cells

Joana Balça-Silva[*,†,‡], Diana Matias[‡,§], Luiz Gustavo Dubois[‡], Brenno Carneiro[§], Anália do Carmo[*,¶], Henrique Girão[*,†], Fernanda Ferreira[§], Valeria Pereira Ferrer[‡], Leila Chimelli[#], Paulo Niemeyer Filho[#], Hermínio Tão[**], Olinda Rebelo[‡‡], Marcos Barbosa[†,], Ana Bela Sarmento-Ribeiro[*,†,‡‡,§§], Maria Celeste Lopes[*,¶¶] and Vivaldo Moura-Neto[#]**

*Center for Neuroscience and Cell Biology and Institute for Biomedical Imaging and Life Sciences (CNC.IBILI), Coimbra, Portugal; [†]Faculty of Medicine, University of Coimbra (FMUC), Coimbra, Portugal; [‡]Instituto Estadual do Cérebro Paulo Niemeyer (IECPN)-Secretaria de Estado de Saúde, Rio de Janeiro, Brazil; [§]Federal University of Rio de Janeiro, Rio de Janeiro, Brazil; [¶]Clinical Pathology Department, Coimbra Hospital and Universitary Center (CHUC), Coimbra, Portugal; [#]Instituto Estadual do Cérebro Paulo Niemeyer (IECPN)-Secretaria de Estado de Saúde, Rio de Janeiro, Brazil; **Neurosurgery Service, Centro Hospitalar Universitário de Coimbra (CHUC), Coimbra, Portugal; [††]Neuropathology Laboratory, Neurology Service, Centro Hospitalar Universitário de Coimbra (CHUC), Coimbra, Portugal; [‡‡]Laboratory of Oncobiology and Hematology and CIMAGO, Faculty of Medicine, University of Coimbra (FMUC), Coimbra, Portugal; [§§]Hematology Department, Centro Hospitalar Universitário de Coimbra (CHUC), Coimbra, Portugal; [¶¶]Faculty of Pharmacy, University of Coimbra (FFUC), Coimbra, Portugal

Abstract

Glioblastoma (GBM) is the most malignant primary brain tumor, with an average survival rate of 15 months. GBM is highly refractory to therapy, and such unresponsiveness is due, primarily, but not exclusively, to the glioma stem-like cells (GSCs). This subpopulation express stem-like cell markers and is responsible for the heterogeneity of GBM, generating multiple differentiated cell phenotypes. However, how GBMs maintain the balance between stem and non-stem populations is still poorly understood. We investigated the GBM ability to interconvert between stem and non-stem states through the evaluation of the expression of specific stem cell markers as well as cell communication proteins. We evaluated the molecular and phenotypic characteristics of GSCs derived from differentiated GBM cell lines by comparing their stem-like cell properties and expression of connexins. We showed that non-GSCs as well as GSCs can undergo successive cycles of gain and loss of stem properties, demonstrating a bidirectional cellular plasticity model that is accompanied by changes on connexins expression. Our findings

Address all correspondence to: Vivaldo Moura-Neto, PhD, Instituto Estadual do Cérebro Paulo Niemeyer (IECPN)- Secretaria de Estado de Saúde, R. do Rezende, 156-Centro, Rio de Janeiro, RJ, 20231-092, Brazil.
E-mail: joanabalca.silva@gmail.com
Received 29 December 2016; Revised 15 April 2017; Accepted 17 April 2017

1936-5233/17
http://dx.doi.org/10.1016/j.tranon.2017.04.005

indicate that the interconversion between non-GSCs and GSCs can be modulated by extracellular factors culminating on differential expression of stem-like cell markers and cell-cell communication proteins. Ultimately, we observed that stem markers are mostly expressed on GBMs rather than on low-grade astrocytomas, suggesting that the presence of GSCs is a feature of high-grade gliomas. Together, our data demonstrate the utmost importance of the understanding of stem cell plasticity properties in a way to a step closer to new strategic approaches to potentially eliminate GSCs and, hopefully, prevent tumor recurrence.

Translational Oncology (2017) 10, 555–569

Introduction

In the last decade, cancer cells endowed with self-renewal, differentiation, and tumor-initiating properties have been isolated from several kinds of malignancies, including central nervous system (CNS) neoplasms. In the brain, glioma stem-like cells (GSCs) have been isolated from primary glioblastomas (GBMs), the most common and malignant primary brain tumor in adults [1–3]. On average, patients with GBM survive only about 15 months after diagnosis even under treatment with temozolomide, which is part of the *gold-standard* therapy [4–7]. This unfavorable prognosis is due to the high proliferation rate, resistance to apoptosis, increased migratory ability of the cells, deregulation of important signaling pathways, and the existence of GSCs. In addition to their potential for tumor initiation, GSCs are responsible for cellular heterogeneity and chemo- and radioresistance, classical features of GBM [8]. This heterogeneity provides several distinct cell populations that differ from each other not only phenotypically but also genetically [9–12] and physiologically [13]. These distinct cell subpopulations produce a rich environment with a sufficient number of cells that can bypass selection pressures to evolve and sustain tumor growth.

The key characteristics of GSCs are suggested to be closely associated with the expression of pluripotency genes, namely, the sex-determining region Y-Box (SOX2) [14].

Nonetheless, a growing body of evidence indicates that intercellular communication through gap junctions could contribute to the coordination of mechanisms involved in cell differentiation [15–18]. Gap junctions are formed by proteins of the connexin (Cx) family, which may exert both tumor-suppressor and oncogenic functions, specifically Cx43 and Cx46 [19,20]. Because the expression of connexins varies according to the differentiation spectrum of GBM cells, Hitomi and colleagues suggested that Cx expression could be essential for transitions between stem-like and non–stem-like states [21]. Switching between stem states allows cells to reprogram their differentiation status and contributes to the development of chemoresistance mechanisms [5,21–23]. However, the mechanisms involved in these cellular transitions and their contributions to GBM chemoresistance and thus aggressiveness are poorly understood [24–27]. Here, we hypothesized that this heterogeneity in GBM tumor mass could represent the reversible transit of GBM cells between different states, such as stem-like and non–stem-like, as a demonstration of glioma stem-like cell plasticity.

Therefore, in order to determine if GBM cells are able to switch between stem and nonstem states, we compared the expression of stem-like markers in GBM cell lines, such as SOX2, upon different culture conditions. Moreover, we compared Cxs expression in such conditions. We also investigated whether the differential expression of SOX2 or Cx can distinguishes glioma grades malignancy through the analysis of human astrocytoma samples. We consider of sublime importance the understanding of stem-like cell state plasticity, which could explain the aggressiveness of GBM and lead us to identify new molecular markers for its treatment.

Material and Methods

Material

Dulbecco's modified Eagle medium/Nutrient Mixture F-12 (DMEM/F12) and NS34 NeuroBasal medium were supplied by Gibco; HEPES was supplied by Life Technologies (São Paulo, Brazil), and fetal bovine serum (FBS) was supplied by Invitrogen (Paisley, UK). The growth factors B27, N2, and G5 were obtained from Thermo Scientific (Waltham, MA). All secondary antibodies conjugated with either Alexa Fluor 488 or Fluor 546 were obtained from Invitrogen–Life Technologies (Carlsbad, CA). Glucose was purchased from Merck (Darmstadt, Germany). Fungizone was purchased from Bristol-Myers Squibb (Princeton, NJ). Penicillin/streptomycin was purchased from Gibco, and rabbit anti–glial fibrillary acidic protein (GFAP) and mouse anti-vimentin clone V9 antibodies were purchased from Dako (Glostrup, Denmark). 4-6-Diamino-2-phenylindole (DAPI) was obtained from Sigma (Natick, MA). Protease and phosphatase inhibitors were supplied by Roche (Indianapolis, IN). Antibodies for Nanog (#3580), Oct-4A (#2840), SOX2 (#D6D9), and Slug (#9585) were purchased from Cell Signaling Technology (Beverly, MA). Mouse GAPDH, anti-Cx43/GJA1 antibody (Cx43) (#ab11370), and anti-GJA3 antibody (Cx46) (#ab176394) were purchased from Abcam. Anti-vimentin was obtained from Dako (Glostrup, Denmark). Mouse anti-actin antibody was purchased from Boehringer (Mannheim, Germany). Nestin clone 10c2 and PVDF membranes were purchased from Millipore (Billerica, MA). 2× Laemmli buffer and β-mercaptoethanol were purchased from Bio-Rad (São Paulo, Brazil).

Maintenance of Cell Line Cultures

The U87 cell line was acquired from the American Type Culture Collection (ATCC) (Manassas, VA). The human tumor cell lines, GBM02 and GBM11 cells, were established and characterized in our laboratory and maintained directly in DMEM/F12 supplemented with bovine serum after being collected from a GBM patient biopsy sample, as previously described [28,29]. The human cell line OB1 was established and characterized by the laboratory of Dr. Hervé Chneiweiss and maintained in NS34 serum-free medium as described by Thirant et al. (2012). Cells were cultured in DMEM supplemented with 3.5 mg/ml of glucose, 0.1 mg/ml of penicillin, 0.14 mg/ml of streptomycin, and 10% inactivated FBS, maintained

at 37°C in an atmosphere containing 95% air and 5% CO_2 as described by Faria et al. (2006). The GSC populations were obtained from U87, GBM02, and GBM11 and maintained in NeuroBasal medium supplemented with sodium pyruvate, glutamine, B27 supplement, epidermal growth factor (EGF), basic fibroblast growth factor (FGF), penicillin, and streptomycin (NS34), as described by Patru et al. [30] and Thirant et al. [31]. Because these cells were obtained in the absence of serum (serum-free, SF), they were termed U87-SF, GBM02-SF, GBM11-SF, and OB1-SF. Spheres from U87-SF, GBM02-SF, GBM11-SF, and OB1-SF were passed by mechanical dissociation through a P200 pipette, reseeded into NS34 medium, and used for stem-like cells at the same density of 0.5×10^6 cells/ml to form new spheres.

Clonogenic Assay

To determine the ability of GBM cells to form spheres, a single viable cell was transferred to each well of a 96-well plate containing 100 µl of NS34 medium. Fresh stem cell medium was added every 2 days. Over 4 weeks of culture, by observation under phase contrast, the sphere-positive wells were counted.

Immunoblotting

The SOX2, OCT-4A, NANOG, Cx43, Cx46, and Slug proteins were analyzed by Western blotting as originally described by Towbin and adapted by Balça-Silva and Kahn in both the GBM and GBM-SF cell lines [28,32,33]. Briefly, cells were centrifuged at 500×*g* for 10 minutes at 4°C. The supernatants were discarded. The cells were resuspended in RIPA buffer (50 mM Tris–HCl at pH 8.0, 150 mM NaCl, 1.0% NP-40, 0.5% sodium deoxycholate, 0.1% SDS, and 2 mM EDTA, supplemented with protease and phosphatase inhibitors and DTT) and sonicated. After that, the samples were denatured with Laemmli buffer 2× added to each sample at a 1:1 ratio. Protein extracts were boiled at 95°C for 5 minutes before use. Thirty micrograms of protein was run on a 10% SDS-PAGE gel, transferred to a PVDF membrane, and then incubated with a solution of 5% nonfat milk in TBST for 1 hour at room temperature. The primary antibodies against SOX2 (1:1000), OCT-4A (1:1000), NANOG (1:1000), Slug (1:1000), vimentin (1:1000), Cx43 (1:1000), and Cx46 (1:100) were diluted in TBST with 1% nonfat milk supplemented with azide. After the incubation period, the immunocomplexes were detected with anti-rabbit antibody (1:1000) and conjugated with horseradish peroxidase. Bands were obtained after exposing the membranes to an X-ray film and analyzed through densitometry scanning. The protein expression was quantified using the software ImageJ 1.49v (Wayne Rasband, National Institutes of Health, Bethesda, MD) with the expression of tubulin or GAPDH used as a loading control. Each experiment was repeated three times.

Immunofluorescence

For immunofluorescence analysis, 10×10^4 cells/ml were plated on coverslips placed on a 24-well plate, as previously described [28]. Briefly, GSCs and GBM cells were fixed with 4% PFA in PBS for 15 minutes. Then, cells were washed with PBS and permeabilized with Triton 0.1% for 30 minutes. Cells were the washed with PBS and incubated with 5% BSA/PBS for 30 minutes. Cells were incubated with rabbit anti-SOX2 (1:400), rabbit anti-GFAP (1:500), rabbit anti–OCT-4A (1:400), rabbit anti-Nanog (1:400), mouse anti-Nestin (1:200), rabbit anti-Cx43 (1:1000), and/or rabbit anti-Cx46 (1:100). Cells were incubated overnight at 4°C with the primary antibodies, then washed again with PBS and incubated overnight with secondary antibodies conjugated with Alexa Fluor 488 (goat anti-mouse; 1:250) and/or Alexa Fluor 488 (goat anti-rabbit; 1:250). Cells were then washed with PBS, stained with DAPI, washed with PBS, and mounted in Fluoromount-G. Negative controls were performed with nonimmune rabbit or mouse IgG. Cells were imaged at 63× using a DMi8 advanced fluorescence microscope (Leica Microsystems, Germany) and analyzed with Leica LA SAF Lite. Images were processed using the software ImageJ 1.49v (Wayne Rasband, National Institutes of Health).

Real-Time Polymerase Chain Reaction (PCR)

Total RNAs were extracted from OB1 and GBM02 cells using PureLink RNA Mini Kit (Thermo Fisher Scientific) following the manufacturer's instructions. One microgram of the total RNA, oligodT(12-18) primer (Thermo Fisher Scientific), and High-Capacity cDNA Reverse Transcription Kit (Applied Biosystems) were used to perform the cDNA synthesis. For quantitative PCR (qPCR) using OB1 cell samples, we utilized 12 ng per well of cDNA, SOX2, and Cx43 Taqman Probes (Hs01053049_s1 and Hs00748445_s1, respectively) and GAPDH (Hs02786624_g1) as endogenous gene. To calculate the relative fold variation in mRNA expression, we performed the $2^{-\Delta\Delta CT}$ method. For qPCR from GBM02 cell samples, we designed and used the SOX2 primers (forward: 5′-AGGGCTGGGAGAAAGAAGAG-3′; reverse: 5′-GGAGAATAGTTGGGGGGAAG-3′), the Cx43 primers (forward: 5′-ATGAGCAGTCTGCCTTTCGT-3′; reverse: 5′-TCTGCTTCAAGTGCATGTCC-3′), and GAPDH (forward: 5′-GAGTCAACGGATTTGGTCGT-3′; reverse: 5′-TTGATTTTG-GAGGGATCTCG-3′) primers. Here, we employed the Power Sybr-Green Master Mix (Thermo Fisher Scientific) and the Pfaffl method of Pfaffl to calculate the relative fold variation in mRNA expression. Data were always obtained from three independent experiments and analyzed using Student's *t* test. Thermal cycling was carried out using the manufacturer's recommended conditions in a CFX96 Touch Real-Time PCR Detector (BioRad) [34].

In Vivo Mouse GBM Model

Swiss mice were obtained from the Biomedical Sciences Institute (Universidade Federal do Rio de Janeiro, Brazil). This study was approved by the Ethics Committee of the Center for Health Sciences (Centro de Ciências da Saúde, Universidade Federal do Rio de Janeiro) (Protocol No. DA-HEICB 015) and by the Brazilian Ministry of Health Ethics Committee (CONEP No. 2340), as described by Kahn et al. [28]. The Guide for the Care and Use of Laboratory Animals (National Academy of Sciences, National Academy Press, Washington, DC) was strictly followed in all experiments. All efforts were made to minimize the number of animals used and their suffering. Ten- to 14-week-old male Swiss mice weighing 20 to 25 g were anesthetized with diazepam (5 mg/kg i.m.), ketamine (100 mg/kg i.m.), and xylazine (25 mg/kg i.m.), and then a brain midline incision was made on the scalp, as previously described [13,28]. Briefly, a small hole was drilled in the skull, and 1×10^5 GBM11 cells (or DMEM/F12; control) were delivered in 3 µl of DMEM-F12 at a depth of 3 mm with a Hamilton syringe (Hamilton, Reno, NV) over 30 minutes at the stereotaxic coordinates: 1 mm posterior to the bregma and +2 mm mediolateral from the midline. Animals were followed for 7, 14, and 21 days after tumor cell injection.

Magnetic Resonance Imaging (MRI)

MRI was performed 7, 14, and 21 days after the tumor injection, as previously described [13,28]. Briefly, mice were anesthetized with ketamine (100 mg/kg i.m.) and xylazine (25 mg/kg i.m.), and images were acquired with a magnetic resonance scanner (7 T/210 horizontal

Varian scanner, Agilent Technologies). All images of the brain were obtained using proton density sequences (repetition time/echo time: 10/2000 ms; matrix: 128 × 128, slice thickness: 1 mm; 12 continuous slices with no gap; 16 averages) in the axial (field of view: 25.6 × 25.6 cm), coronal (field of view: 32 × 32 cm), and sagittal (field of view: 25.6 × 25.6 cm) planes. For each data set, all images were visually inspected for artifacts. Data were processed using Osirix software (www.osirix-viewer.com). Brain morphology and tumor characteristics were evaluated by two experienced researchers.

Mouse Tissue Processing

Briefly, mice brains were dissected, fixed in 4% PFA for 24 hours at 4°C, and stored before processing. Then, the tissues were dehydrated in a graded ethanol series (30%, 40%, 50%, and 60% for 30 minutes; next 70%, 80%, and 90% for 1 hour; and finally 100% twice for 1 hour each), followed by xylene overnight at room temperature. Finally, brains were embedded in paraffin for 3 hpurs at 67°C. Coronal sections were cut (5 μm thick) on a microtome. The sections were stained with hematoxylin and eosin and photographed using a DMi8 advanced fluorescence microscope (Leica Microsystems, Germany). For immunofluorescence of GBM11 cells injected in the striatum of immunocompetent mice, mouse anti-human vimentin (hVim) (1:50) was stained at the core of the tumor mass, as shown by cell nuclei atypia (DAPI counterstaining in cyan, inset), and at the border of the tumor mass.

Human Tissue Processing

A total of 10 human brain samples, of which 6 were astrocytoma grade IV (GBM), 2 astrocytoma grade II, and 2 temporal lobectomy neocortex samples, acquired from epilepsy surgery patients with mesial sclerosis were considered as normal brain and used as controls were collected. All patients were admitted to the Neurosurgery Service of the University Hospital of Coimbra (Coimbra, Portugal). The study was approved by the University Hospital of Coimbra Ethics Committee according to the Declaration of Helsinki protocol, and all patients signed an inform consent for the use of biological material for research investigation. The GBM, astrocytoma grade II, and normal brain tissues were fixed in 4% paraformaldehyde for 12 to 24 hours, embedded in paraffin, and cut into 4-μm sections. The brain tissues were prepared for immunohistochemistry by deparaffinizing the sections in xylene for 20 minutes and rehydrating in an ethanol series using a Vector Laboratories (Burlingame, CA) VP-P980, clone PC10 (IgG2a) kit. Then, all sections were incubated for 30 minutes with 3% H_2O_2. Antigens were retrieved from the samples with citric acid buffer (citric acid 0.1 M and sodium citrate 0.1 M in distilled water) in a microwave (two cycles of 5 minutes, 400 W) to break the methylene bonds and expose the antigenic sites. After that, the sections were incubated in horse normal serum (Vector Laboratories) at 4°C for 30 minutes and then incubated with SOX2 primary antibody (1:100) diluted in TBS overnight at 4°C. The sections were washed three times with TBS-Tween and next incubated with a 1:100 secondary antibody ImmPress reagent (Vector Laboratories Anti-mouse/rabbit Ig, cat. no. MP-7500) for 30 minutes at room temperature. Then, all sections were incubated with diaminobenzidine (Bios, Beijing, China) for visualizing the positive signal, counterstained with Mayer's hematoxylin, and evaluated and scored by two independent pathologists (with no knowledge of the patients' records). The sections were observed at the same magnification of 10× (×10/0.25 PH1 NPLAN) and amplified 40× (×40/0.55 CORR PH2) (scale bar = 100 μm) with a Leica DMI3000B light microscope (Leica, Germany) and acquired with the Leica Application Suite v 4.3 (Leica, Switzerland).

Statistical Analysis

Statistical analysis was performed in GraphPad Prism 5 for Windows, version 5.00 (GraphPad Software, Inc., San Diego, CA). After the assumption of normality and homogeneity of variance across groups was confirmed, the groups were compared using a nested design with analysis of variance and *post hoc* comparison, with correction of α error according to Bonferroni probabilities to compensate for multiple comparisons. All values were expressed as mean ± SEM, $P < .05$.

Results

GBM Cell Lines Interconvertion Between Stem-Like and Non–Stem-Like States

GBM can generate cells that are able to acquire the stem-like state independently of their differentiation state [23]. Two different GBM cell lines, which were isolated by different methods, were cultured in different media. GBM02 was derived from an adult human patient and isolated directly in medium supplemented with fetal bovine serum (DMEM-F12, 10% FBS). OB1-SF (OB1–serum-free) was isolated from an adult human patient and first cultured in a defined growth media supplemented with growth factors (NS34, which contains DMEM/F12 5×; glucose 30%; 200 mM glutamine; HEPES 3.6%; $NaHCO_3$ 7.5%; Pen/Strep; N2 1×; B27 1×; and G5 1×), known for maintaining stem-like properties [3,31]. Specifically, the N2 is constituted by human transferrin, human insulin, progesterone, putrescine, and sodium selenite and is recommended for the growth and expression of neuroblastomas [35]. The B27 is composed by a cocktail of vitamins, proteins, and other components like linoleic acid, linolenic acid, progesterone, and selenite sodium, among others. The B27 is used to induce growth and long-term viability of CNS cells [36]. Finally, the G5 is composed by biotin, basic FGF, EGF, human transferrin, and human insulin, among others, and is also important to the growth and maintenance of primary and tumor glial cells [35]. To investigate whether the two cell lines can switch between stem-like and non–stem-like states, the expressions of SOX2 and Cxs 43 and 46 were measured by Western blot (WB), when the cells were cultured in their respective media, for both GBM02 (Figure 1*A*, T0) and OB1-SF (Figure 2*A*, T0). The expressions of SOX2, Cx43, and 46 were also evaluated by immunocytochemistry (ICC) (Figures 1*B* and 2*B*) and by qPCR (Figures 1*C* and 2*C*). Two weeks later, cell differentiation was induced in the OB1 cell line by exposing the cells to DMEM-F12 10% SFB, and reacquisition of stem-like properties in GBM02 (GBM02-SF) was induced by exposure to NS34 medium. The expression of markers of the stem-like state was assessed by WB, ICC, and qPCR (Figures 1 and 2). At the end of 4 weeks, the GBM02 cells were transferred back to the DMEM-F12 10% SFB medium, and the OB1-SF cells were transferred back to the NS34 medium (Figures 1 and 2, T4). Our results showed that after this transfer, in the GBM02 cells (T4), the Cx43 protein amount was 4.3-fold higher than in the GBM02-SF cells (T2), $P < .01$ (Figure 1*A*). However, there was no significant difference among the Cx43 mRNA expression analyzed (Figure 1*C*). The GBM02-SF cells (T2) maintained the ability to form spheres, and the Cx46 protein was 4.0-fold higher than in the GBM02 cells (T0), $P < .05$, and 6.0-fold higher than in the GBM02 cells (T4), $P < .05$. In

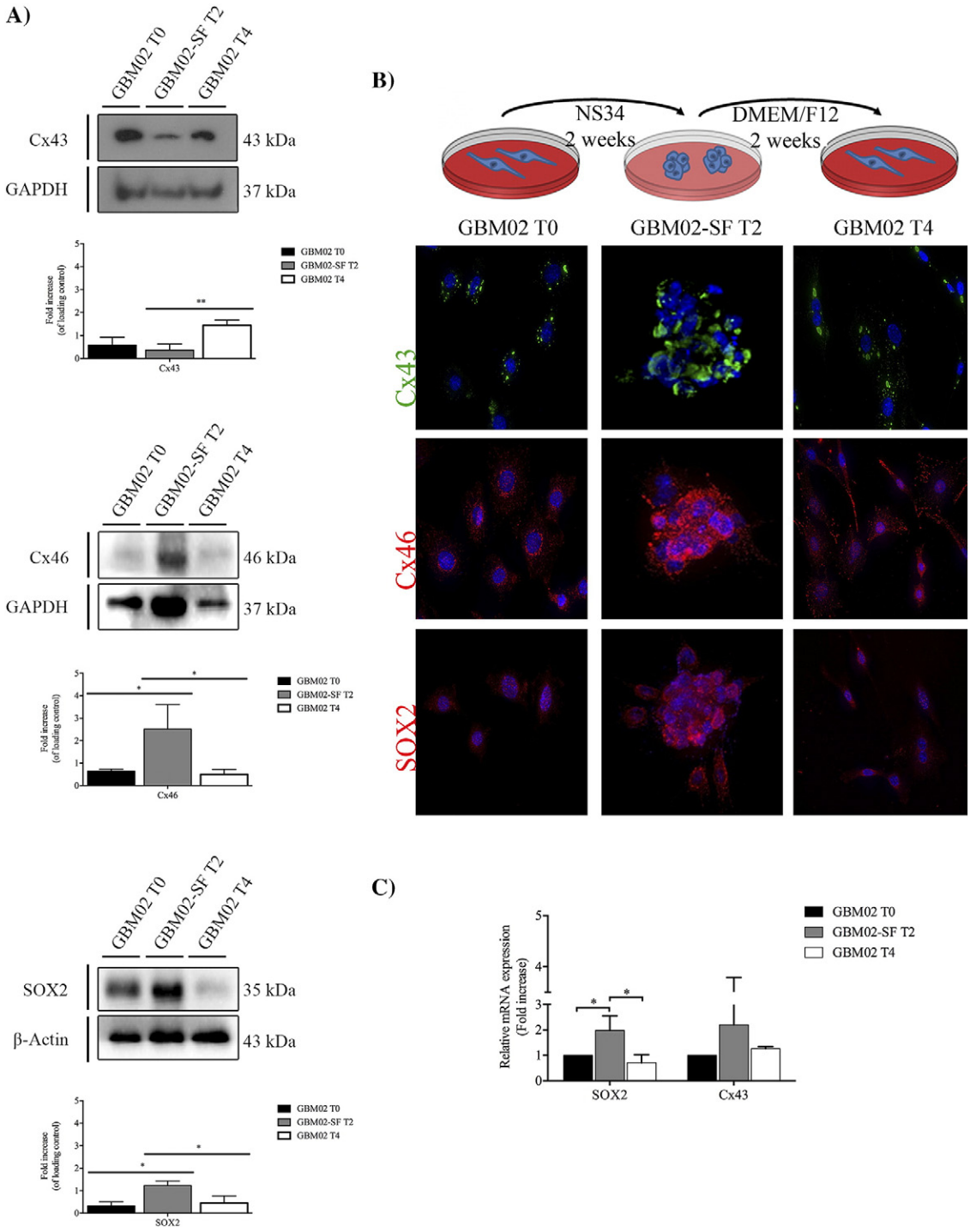

Figure 1. GBM stem-like cell plasticity properties in GBM02 and GBM02-SF cells. The expression of Cx43, Cx46, and SOX2 in the GBM and the respective serum-free cell lines was evaluated by WB (A) and immunofluorescence (B). (A) GBM02 cells were maintained in DMEM-F12 supplemented with serum for 2 weeks (GBM02 T0). At the end of this time, part of the cells was isolated and the other part was maintained in culture with NS34, a serum-free medium, for 2 more weeks (GBM02-SF T2). Next, part of the cells was also isolated and the other part was again maintained in culture with DMEM/F12 supplemented with serum for a further 2 weeks (GBM02 T4). At the end of this time, cells were collected, and the expression of Cx43, Cx46, and SOX2 was quantified by WB as previously described. Statistical analysis was performed in GraphPad Prism 5 for Windows (version 5.00; GraphPad Software, Inc., San Diego, CA). Each value represents the mean ± SEM from three independent experiments; $*P < .05$, $**P < .01$. (B) Immunofluorescence staining of Cx43, Cx46, and SOX2 was performed in parallel. Cells were imaged at 63× magnification using a DMi8 advanced fluorescence microscope (Leica Microsystems, Germany) and analyzed with Leica LA SAF Lite. Images were processed using the software ImageJ 1.49v (Wayne Rasband, National Institutes of Health). (C) The expression of Cx43 and SOX2 in the GBM02 and GBM02-SF cells was evaluated by qPCR. Total RNA was extracted using a PureLink RNA Mini Kit following the manufacturer's instructions. One microgram of total RNA, oligo(dT) primer, and High-Capacity cDNA Reverse Transcription Kit were used to perform cDNA synthesis. The qPCR reaction was done in duplicate using SOX2, Cx43, and GAPDH primers and Power SybrGreen Master Mix. To calculate the relative fold variation in mRNA expression, GBM02 cells (T0) were applied as control at the $2^{-\Delta\Delta CT}$ method. Each value represents the ± SEM, $*P < .05$.

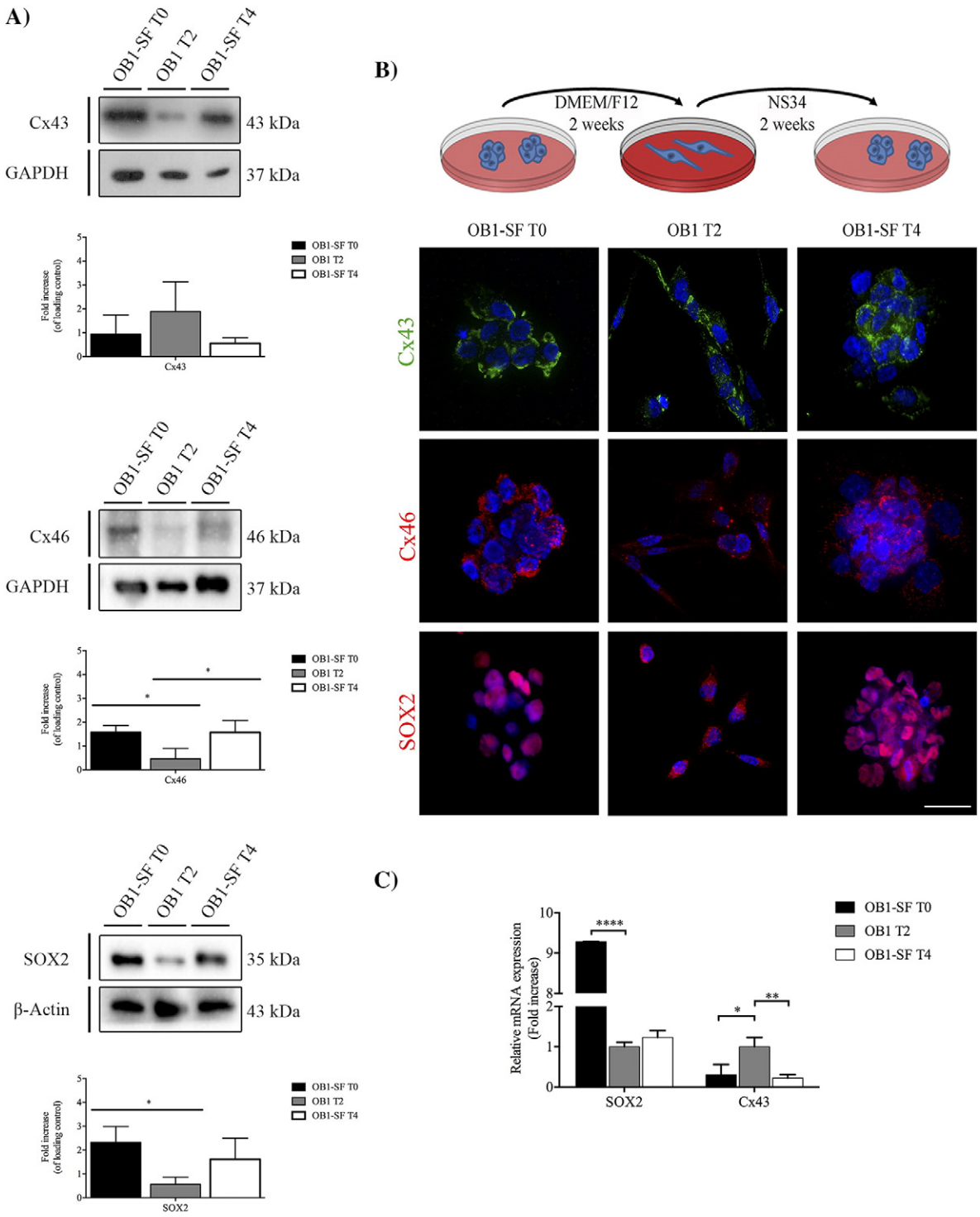

Figure 2. GBM stem-like cell plasticity properties in OB1 and OB1-SF cells. The expression of Cx43, Cx46, and SOX2 was analyzed in the GBM, and the respective serum-free cell lines were evaluated by WB (A) and immunofluorescence (B). (A) OB1-SF cells were maintained in culture with the serum-free medium NS34 for 2 weeks (OB1-SF T0). At the end of this time, part of the cells was isolated and the other part was maintained in DMEM-F12 supplemented with serum for 2 more weeks (OB1 T2). After this time, part of the cells was also isolated and the other part was again maintained in culture with NS34, a serum-free medium, for a further 2 weeks (OB1-SF T4). At the end of this time, cells were collected, and the expression of Cx43, Cx46, and SOX2 was quantified by WB as previously described. Statistical analysis was performed in GraphPad Prism 5 for Windows (version 5.00; GraphPad Software, Inc., San Diego, CA). Each value represents the mean ± SEM from three independent experiments; $*P < .05$, $**P < .01$. B. Immunofluorescence staining of Cx43, Cx46, and SOX2 was performed in parallel. Cells were imaged at 63× magnification using a DMi8 advanced fluorescence microscope (Leica Microsystems, Germany) and analyzed with Leica LA SAF Lite. Images were processed using the software ImageJ 1.49v (Wayne Rasband, National Institutes of Health). (C) The expression of Cx43 and SOX2 in OB1-SF and OB1 cells was evaluated by qPCR. Total RNA was extracted using PureLink RNA Mini Kit following the manufacturer's instructions. One microgram of total RNA, oligo(dT) primer, and High-Capacity cDNA Reverse Transcription Kit were used to achieve cDNA synthesis. The qPCR reaction was done in duplicate using SOX2, Cx43, and GAPDH Taqman Probes. To calculate the relative fold variation in mRNA expression, OB1 cells (T2) were used as control at the $2^{-\Delta\Delta CT}$ method. Each value represents the mean ± SEM; $*P < .05$, $**P < .01$, $****P < .0001$.

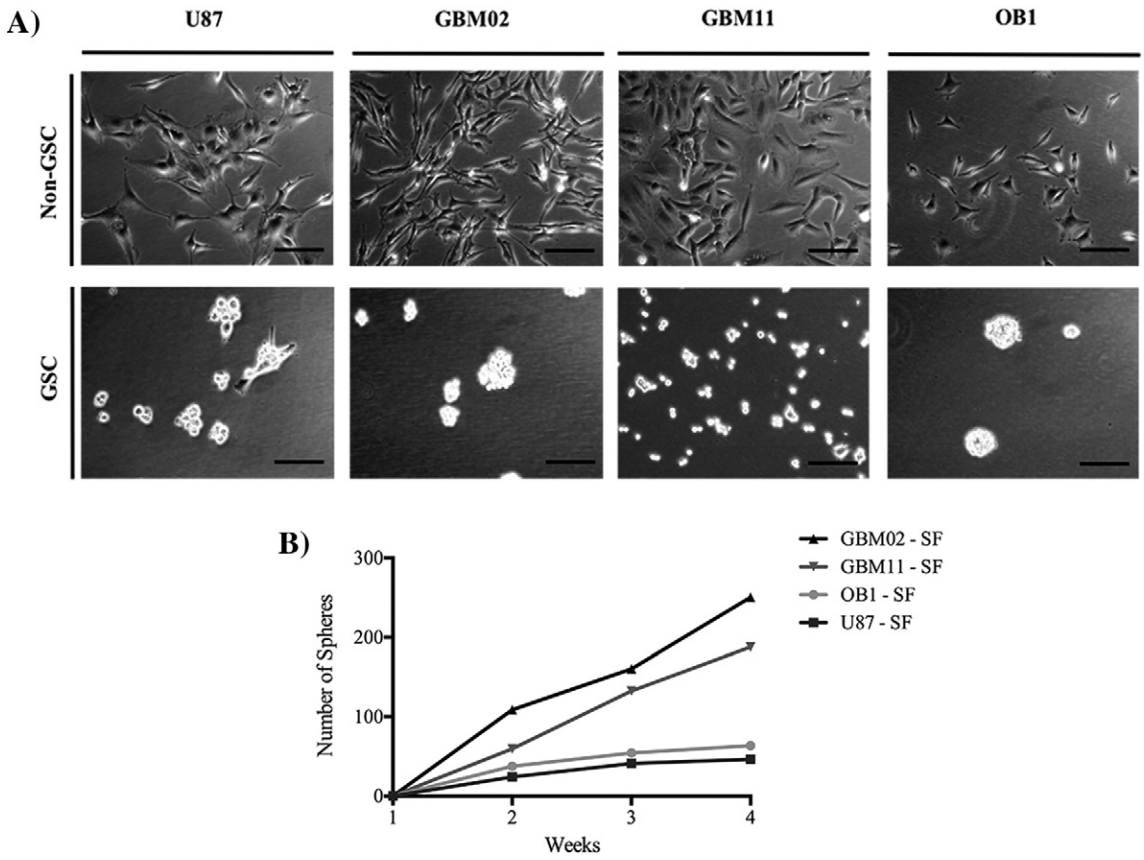

Figure 3. The GSC maintenance (A) and clonogenic Assay (B). (A) The human tumor cell lines were established in our laboratory. The use of patients' surgical specimens for the establishment of cell lines for *in vitro* and *in vivo* studies had written informed consent from the patients and was approved by the Brazilian Ministry of Health Ethics Committee under Institutional Review Board (Research Ethics Committee of Hospital Universitário Clementino Fraga Filho) consent, CEP-HUCFF no. 002/01. Cells were grown and maintained in DMEM-F12 supplemented with 10% FBS. Culture flasks were maintained at 37°C in a humidified 5% CO_2 and 95% air atmosphere. GSCs were maintained as tumor-sphere cultures in NeuroBasal medium supplemented with sodium pyruvate, glutamine, B27 supplement, EGF, basic FGF, penicillin, and streptomycin. The OB1 differentiated cell line was obtained by the removal of EGF and bFGF and the addition of 10% fetal bovine serum. (B) To estimate stem cell frequency in the cell population, tumor-sphere formation was assayed with 2 cells per well in in 96-well plates in NeuroBasal medium supplemented with sodium pyruvate, glutamine, B27 supplement, EGF, basic FGF, penicillin, and streptomycin. During 4 weeks of culture, sphere-positive wells were scored by observation under an inverted microscope with phase-contrast optics. The image is representative of three independent experiments. Cells were imaged at 63× magnification using a DMi8 advanced fluorescence microscope (Leica Microsystems, Germany) and analyzed with Leica LA SAF Lite. Images were processed using the software ImageJ 1.49v (Wayne Rasband, National Institutes of Health).

addition, the quantity of SOX2 in the GBM02-SF cells (T2) was 3.6-fold higher than in the GBM02 cells (T0), $P < .05$, and 2.8-fold higher than in the GBM02 cells (T4), $P < .05$ (Figure 1, *A* and *B*). Corroborating this, the qPCR results showed that SOX2 expression was 1.98 higher in the GBM02-SF cells (T2) than in GBM02 cells (T0), $P < .05$. In addition, statistically, the same mRNA expression value was found in GBM02 cells (T4 and T0) (Figure 1*C*). In the OB1 cells (T2), the expression of Cx43 was higher than that observed in the OB1-SF cells (T0 and T4). The mRNA expression was more than three-fold higher in T2 compared with T0, $P < .05$, and T4 condition, $P < .01$, although the difference was not statistically significant for the protein amount. In the OB1-SF cells (T0), the expression of Cx46 was 3.9-fold higher than in OB1 cells (T2), $P < .05$; and in the OB1-SF cells (T4), the expression of Cx46 was 3.8-fold higher than in the OB1 cells (T2), $P < .05$. In the OB1-SF cells (T0), the total of SOX2 protein was 4.5-fold higher than in the OB1 cells (T2), $P < .05$; and in the OB1-SF cells (T4), SOX2 expression was 3.0-fold higher than in the OB1 cells (T2), although this difference was not statistically significant (Figure 2*A*). Similar results were found for the real-time PCR. SOX2 expression was 9.28 higher in OB1-SF cells (T0) than in OB1 cells (T2), $P < .001$; and the transcripts levels increased in T4 compared with T2 were not statistically significant (Figure 2*C*). Also, the OB1 cells formed spheres when cultured in the stem-like serum-free medium (Figure 2*B*).

Currently, several studies demonstrate that the shifts in the stem-like properties are accompanied by changes in expression of epithelial-mesenchymal transition (EMT) markers [26,37]. We investigated the expression of Slug and Vimentin, two markers of enhanced EMT [38,39], on OB1 cells in three different time points (Supplementary Data 1). Slug and vimentin expression was downregulated on cells cultured on differentiation conditions (OB1-T2) when compared to OB1-SF (T0). On the other hand, their expression was restored when the same population of OB1 cells was cultured back on serum-free media (OB1-T4), $P < .05$ (Supplementary Data 1).

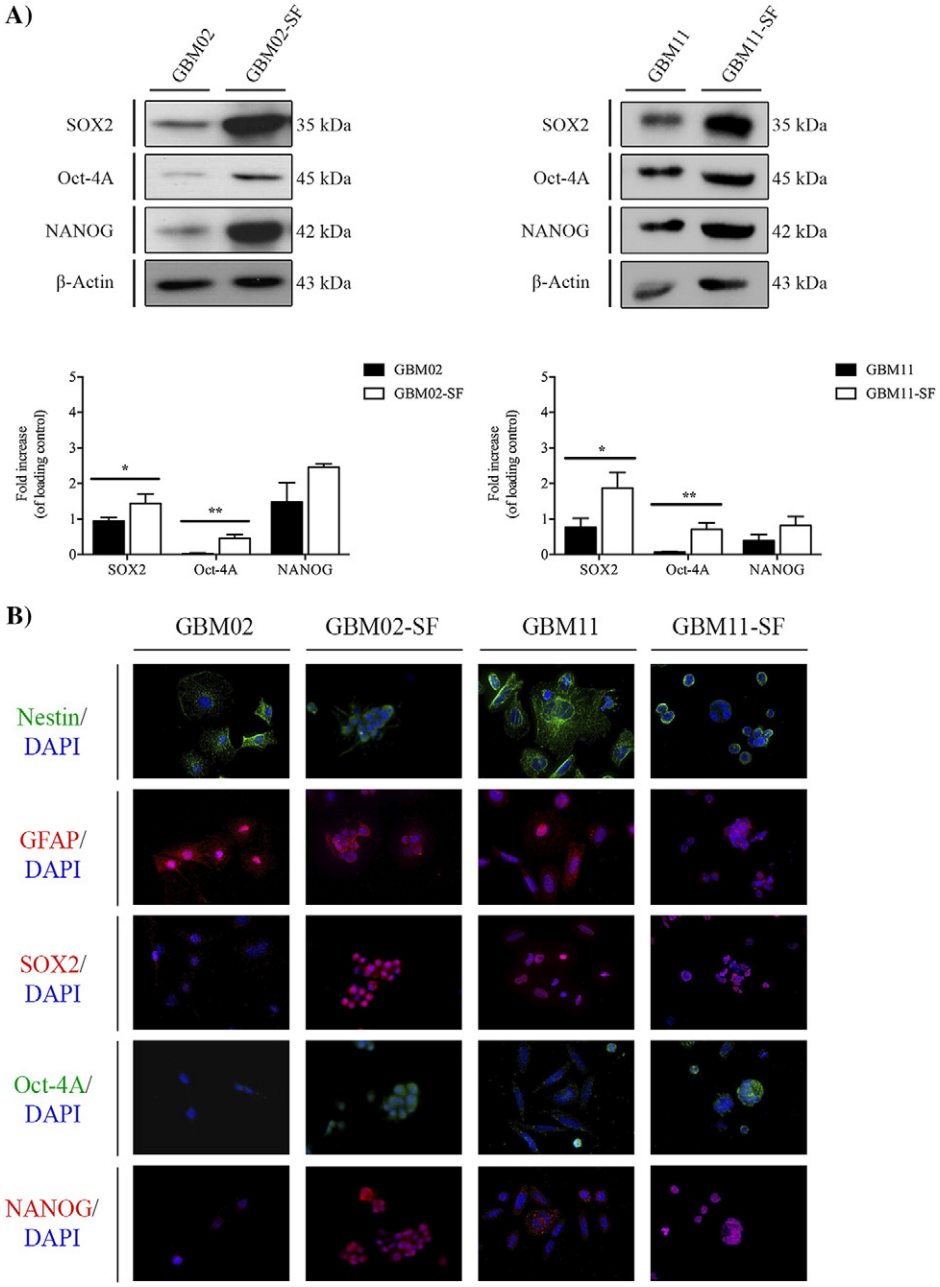

Figure 4. Stem-like cell marker expression in two GBM cell lines isolated from patients in DMEM/F12 supplemented with serum by WB (A) and immunofluorescence (B). (A) The expression of SOX2, OCT-4A, and Nanog in both the GBM02 and GBM11 cell lines, isolated from GBM diagnosed patients, and the respective serum-free GBM cells, as previously described, was quantified by WB. Statistical analysis was performed in GraphPad Prism 5 for Windows (version 5.00; GraphPad Software, Inc., San Diego, CA). Each value represents the mean ± SEM from three independent experiments; $*P < .05$, $**P < .01$. (B) Immunofluorescence staining of SOX2, OCT-4A, and Nanog as well as Nestin and GFAP was performed in both the GBM02 and GBM11 cell lines and the respective serum-free GBM cells, GBM02-SF and GBM11-SF. Cells were imaged at 63× magnification using a DMi8 advanced fluorescence microscope (Leica Microsystems, Germany) and analyzed with Leica LA SAF Lite. Images were processed using the software ImageJ 1.49v (Wayne Rasband, National Institutes of Health).

GSCs Clonogenic Properties

We observed that GBM02 cultured in DMEM/F12 with serum could enhance the expression of stem-like markers after culturing in NS34. This observation prompted us to investigate whether other GBM cell lines previously cultured in serum-supplemented media could acquire stem-like properties when cultured in NS34. The U87, GBM02, and GBM11 cell lines were transferred to the serum-free stem cell medium NS34 (U87-SF; GBM02-SF and GBM11-SF), and their ability to form clones was evaluated. OB1-SF was used as a control because it was already a GSC cell line. Single cells divided within 3 days, followed by the formation of small "oncosphere-like" structures at the end of 1 week. Each sphere contained approximately four cells per sphere. The cells in the U87-SF culture formed spheres containing approximately four cells each, and the GBM02-SF and GBM11-SF

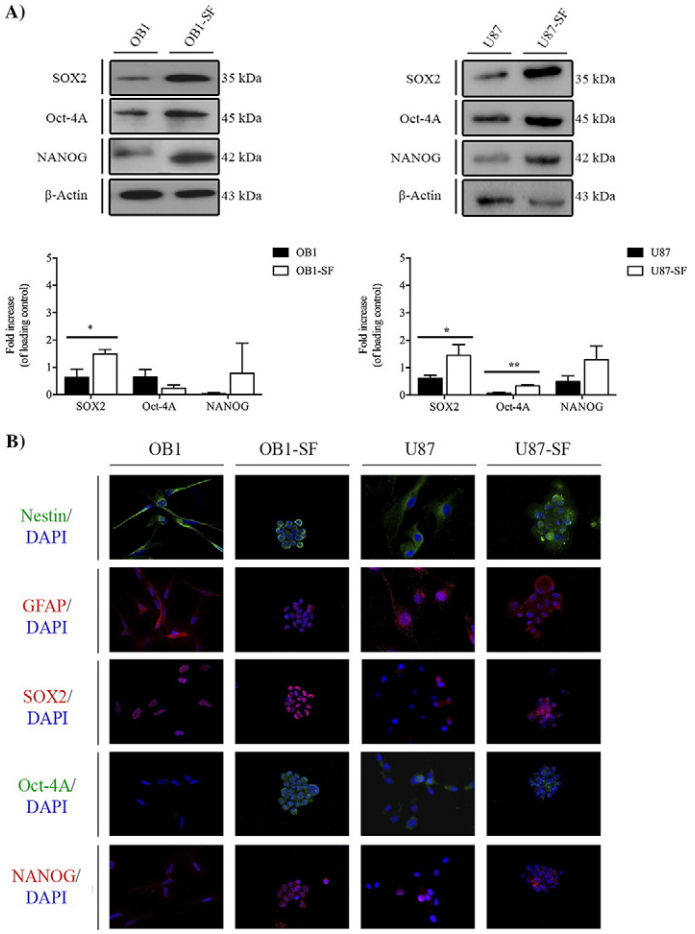

Figure 5. Stem-like cell marker expression in the U87 ATCC GBM cell line and the OB1, a GBM cell line isolated from a patient directly in NS34 serum-free medium, by WB (A) and immunofluorescence (B). (A) The expression of SOX2, OCT-4A, and Nanog was quantified in both the OB1 cell line isolated from a GBM diagnosed patient directly in NS34 serum-free medium and in U87, a GBM cell line acquired by ATCC. The respective OB1 differentiated cells were isolated from OB1-SF, and the serum-free GBM cells were isolated from the U87 cell line, U87-SF, as previously described, by WB. Statistical analysis was performed in GraphPad Prism 5 for Windows (version 5.00; GraphPad Software, Inc., San Diego, CA). Each value represents the mean ± SEM from three independent experiments; $*P < .05$, $**P < .01$. B. Immunofluorescence staining of SOX2, OCT-4A, and Nanog as well as Nestin and GFAP was performed in both the OB1 and U87 cell lines and the respective serum-free GBM cells, OB1-SF and U87-SF. Cells were imaged at 63× magnification using a DMi8 advanced fluorescence microscope (Leica Microsystems, Germany) and analyzed with Leica LA SAF Lite. Images were processed using the software ImageJ 1.49v (Wayne Rasband, National Institutes of Health).

cultures formed spheres containing four to eight cells each. After 2 weeks of culture, observation with a phase-contrast microscope showed that oncospheres had formed, and these were maintained until they reached the maximum size of 200 μm (Figure 3*A*). The spheres were then dissociated, and 0.5×10^6 cells were transferred to a new flask with new NS34 medium in order to evaluate the formation of new spheres, which occurred 1 week later. Serial passage in NS34 medium revealed that the oncospheres maintained the self-renewing ability after at least four generations. We then evaluated the ability of stem-like cells to form new clones by clonogenic assay (Figure 3*B*). In a limited-dilution assay, oncospheres were dissociated into a suspension of single cells, and 1 cell was reseeded into each well of 96-well plates. At the end of each week, the number of spheres was quantified. We found that the GBM02-SF culture cells were better able to form tumor spheres than the GBM11-SF (1.3-fold difference; $P = .2$), OB1-SF (3.9-fold difference; $P < .05$), and U87-SF cells (5.4-fold difference; $P < .01$). On other hand, GBM11-SF demonstrated a better ability to form spheres than OB1-SF (2.9-fold difference; $P < .01$) and U87-SF (4.0-fold difference; $P < .01$). However, the OB1-SF cells were better able to form spheres than the U87-SF cells (1.3-fold difference; $P < .01$) (Figure 3*B*). As so, GBM11-SF has a higher capability to form spheres compared to the other cell lines.

GSCs Expression of Stem-Like State Markers

In order to determine whether the ability of GSCs derived from previously serum-cultured GBM cell lines to form spheres was accompanied by an increase in the expression of stem-like markers, the expression of SOX2, OCT-4A, and NANOG was evaluated using WB (Figures 4*A* and 5*A*) and immunofluorescence (Figures 4*B* and 5*B*). In parallel, the GFAP and Nestin, a type VI intermediate filament protein that is expressed mostly in precursor of nervous cells, were also evaluated by immunofluorescence analysis (Figures 4*B* and 5*B*). The results showed that, in the GBM02-SF cells, the expression of SOX2 was 1.75-fold higher, $P < .05$; the expression of OCT-4A was 43-fold higher, $P < .01$; and the expression of NANOG was 1.7-fold higher, $P < .01$, compared to their expression in the GBM02 cells (Figure 2*A*). In the GBM11-SF cells, the expression of SOX2 was 2.6-fold higher, $P < .05$; the expression of OCT-4A was 15.8-fold higher, $P < .01$; and the expression of NANOG was 2.6-fold higher, $P < .01$, compared to their expression in GBM11 (Figure 4*A*). In the OB1-SF cells, only the expression of SOX2 and NANOG was increased compared to their OB1 cells (2.9-fold higher, $P < .05$ and 2.5-fold higher, $P < .01$, respectively) (Figure 5*A*). Finally, in the U87-SF cells, the expressions of SOX2, OCT-4A, and NANOG were 2.8-, 5.0-, and 3.0-fold higher than in U87 cells ($P < .05$, $P < .01$, and $P < .01$), respectively (Figure 5*A*).

Connexins 43 and 46 Expression During Transition of GBM Cells Between Stem-Like and Non–Stem-Like States

Due to the particular functions of gap junctions in the coordination of many cellular processes, mainly cell proliferation, survival, differentiation, and chemoresistance, we compared the expression of connexins, particularly Cx43 and Cx46, in the DMEM/F12 10% SFB or NS34-cultured GBM cell lines using WB (Figure 6*A*) and ICC (Figure 6*B*) [40]. Our results showed that, in the GBM02 cells, the Cx43 expression was higher than in the GBM02-SF cells; and the Cx46 expression was 12.0-fold higher in the GBM02-SF cells than in the GBM02 cells, $P < .001$. In the GBM11 cells, the Cx43 expression was 1.5-fold higher than in the GBM11-SF cells, although with no statistical significance; the Cx46 expression was 4.0-fold higher in the GBM11-SF cells than in the GBM11 cells, $P < .05$. In the OB1 cells, the Cx43 expression was 5.3-fold higher than in the OB1-SF cells, $P < .01$; and the Cx46 expression was 1.6-fold higher in OB1-SF than in the OB1 cells, although with no statistical significance. Finally, in the U87 cell line, the Cx43 expression was 0.8-fold higher than in the U87-SF cells, with no statistical significance; and the Cx46 expression was 1.3-fold higher in the

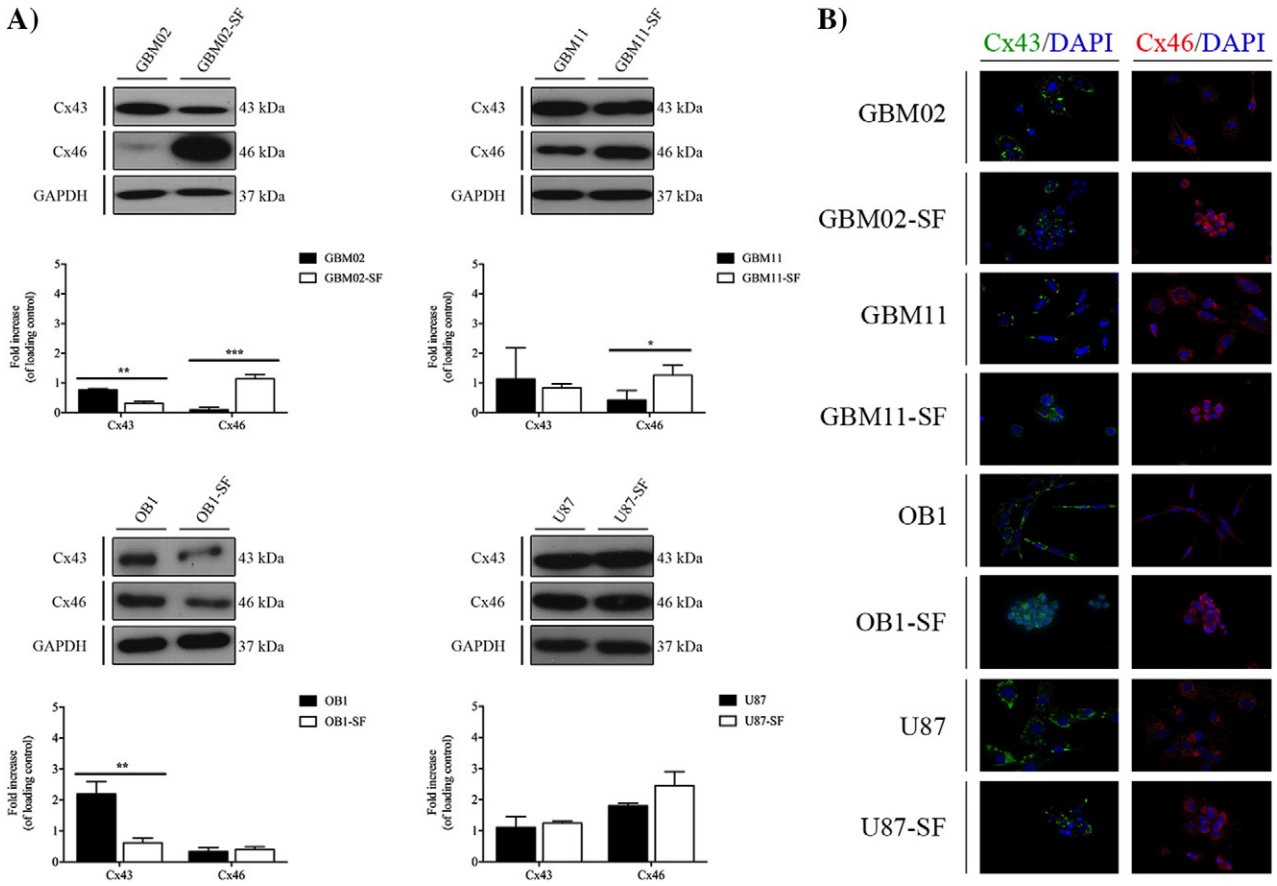

Figure 6. Cx43 and Cx46 expression analysis in the GBM and the respective serum-free cell lines (GSCs) by WB (A) and immunofluorescence (B). (A) The expression of Cx43 and Cx46 in the GBM02, GBM11, OB1, and U87 cell lines and the respective serum-free cells, GBM02-SF, GBM11-SF, OB1-SF, and U87-SF, as previously described, was quantified by WB. Statistical analysis was performed in GraphPad Prism 5 for Windows (version 5.00; GraphPad Software, Inc., San Diego, CA). Each value represents the mean ± SEM from three independent experiments; $*P < .05$, $**P < .01$. (B) Immunofluorescence staining of Cx43 and Cx46 was also performed in all cell lines. Cells were imaged at 63× magnification using a DMi8 advanced fluorescence microscope (Leica Microsystems, Germany) and analyzed with Leica LA SAF Lite. Images were processed using the software ImageJ 1.49v (Wayne Rasband, National Institutes of Health).

U87-SF cells than in the U87 cells, with no statistical significance (Figure 6, *A* and *B*). Overall, accordingly to what is described in literature, our results showed, for the first time, that the Cx43 is overexpressed in non-GSCs, whereas Cx46 is overexpressed in GSCs [40].

Human Glioblastoma Xenograft Growth in Immunocompetent Mouse Brain

A major feature of GSCs is the ability to form a new tumor when xenografted into a mouse brain [2], and GBM cells appear to transit between stem-like and non–stem-like states. This observation led us to xenograft GBM cell lines into mouse brains in order to evaluate whether the cells can form new tumors even when they are not in the stem-like state. GBM11 cells were grafted into the striatum of Swiss mice as previously described [13] (Figure 7*A*). Fourteen days after the tumor cells were injected, MRI was performed to mice brains, and mice were subsequently euthanized (Figure 7*B*). The tumor mass was analyzed macroscopically, revealing a hemorrhagic and necrotic area in the core of the tumor. The histological examination revealed the existence of a lymphoproliferative infiltrate and the presence of mitotic cells (Figure 7*C*). To confirm that the tumor developed due to the proliferation of the injected human GBM11 cells, infiltrating human cells were identified with a mouse anti-human vimentin antibody derived from V9, which showed positive staining (Figure 7*D*). Finally, to confirm the presence of GSCs in the tumor mass, the cells were stained with SOX2, which revealed SOX2-positive cells (Figure 7*D*). Taken together, this evidence suggests that the stem state is dynamic and can be induced depending on the environment where the tumor cell is immersed.

SOX2 and Cx46 Expression in Human Glioma Samples

Because we had determined that the expression of the stem-like cell markers SOX2 and Cx46 mostly changes according to the stem and nonstem state, we next evaluated the expression of SOX2 and Cx46 in tumor sections obtained from a grade II astrocytoma and a grade IV astrocytoma (GBM), comparing with the temporal lobectomy neocortex samples acquired from epilepsy surgery patients with mesial sclerosis considered as normal brain, as described in the Material and Methods section. Comparing to astrocytoma grade II that presented microcysts and nuclear atypia, in GBM, we observed a nuclear atypia, prominent microvasculature proliferation (+), and necrosis (*), which constitute the essential diagnostic features of GBM (Figure 8*A*). In the immunohistochemistry analysis, the tumor sections obtained from the grade IV astrocytoma showed a higher SOX2 and Cx46 expression than in the tumor sections from the grade II astrocytoma

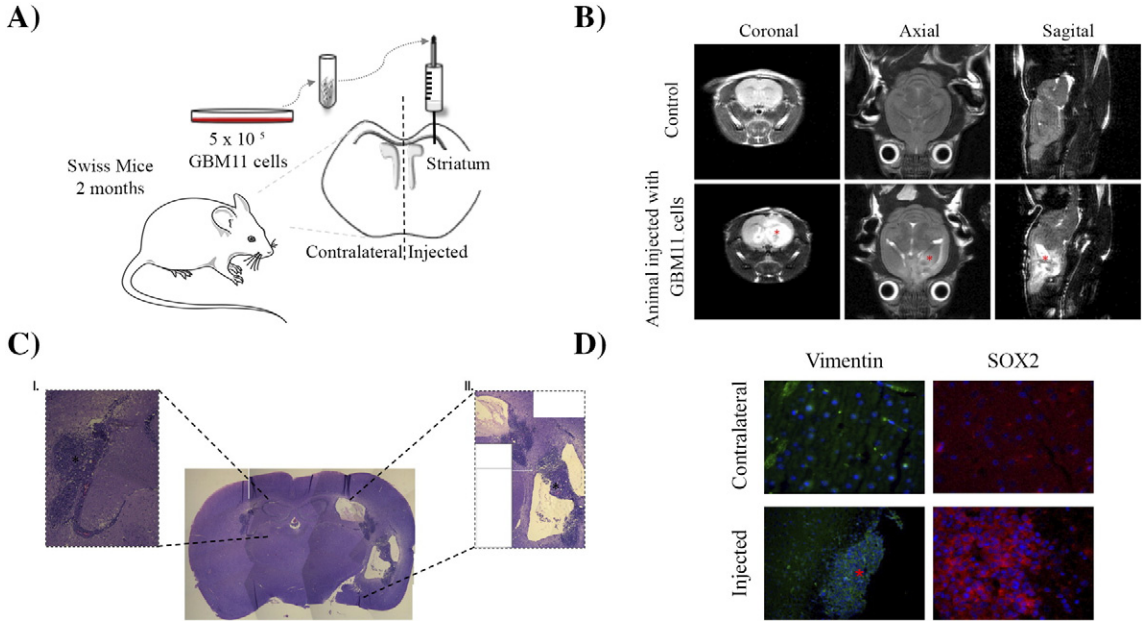

Figure 7. Capability of GBM cell lines to form tumors *in vivo*. (A) Schematic depiction of GBM11 cell injection in striatum region of immunocompetent Swiss mouse brain. (B) MRI 14 days after GBM11 cell transplantation into a representative mouse brain. Coronal, sagittal, and axial cuts of tumor site in control and GBM11-injected mice. The asterisk (*) indicates the tumor mass. (C) Histopathological characteristics of the tumor mass in mouse brain parenchyma 14 days after implantation of GBM11 cells, revealed by hematoxylin-eosin staining. I: Neoplastic cells forming a circumscribed solid tumor mass in the brain tissue (black asterisk). II: Glomeruloid vessels (black asterisk). Microscopic analysis showed anaplastic cells and tumoral necrosis. (D) Immunohistochemical characteristics of the tumor revealed the expression of human vimentin (hVim). hVim staining (green) at the core of the tumor mass (red asterisk) and SOX2 (red), depicted by cell nuclei atypia (DAPI counterstaining in cyan blue, inset), and at the border of the tumor mass. Cells were imaged at 63× magnification using a DMi8 advanced fluorescence microscope (Leica Microsystems, Germany) and analyzed with Leica LA SAF Lite. Images were processed using the software ImageJ 1.49v (Wayne Rasband, National Institutes of Health).

and from normal patients, which suggest that the occurrence of GSCs is linked to the grade of the glioma [29,30](Figure 8, *B* and *C*).

Discussion

GBM is the most common and fatal type of primary brain tumor [1,41–43]. In spite of recent advances, GBM treatment remains palliative, mainly due to the occurrence of chemo- and radioresistant GSCs, which contribute to tumor growth, metastasis, and relapse [8,14,44,45]. As such, GSCs have become a main focus of GBM therapeutic research. Previous studies revealed that GSCs may emerge from the increased self-renewing division of GSCs or from reprogramming of non-GSCs to GSCs, maybe suggesting a plasticity of the stem state in GBM [23]. We considered that the understanding of GBM stem state plasticity is of utmost importance to identify the mechanisms and factors involved in GSCs' resistance to therapy, which may justify tumor recurrence and so constitute a step forward to the identification of new approaches to treat GBM.

It is well known that GSCs can lose their stem-like properties, giving rise to non-GSCs, but is the reverse true? Previous studies have suggested that GSC plasticity could be dynamic and that both GSCs and non-GSCs are capable of switching their status [23]. Moreover, GSC interactions with the surrounding microenvironment could determine GBM heterogeneity and dictate the balance between self-renewal and differentiation properties [21]. Here, using GBM cell lines and patient samples, we identified molecular markers that could translate both states in GBM (Figures 1 and 2). Our results showed that non-GSCs, obtained from culturing in DMEM/F12 with serum-supplemented medium, expressed less SOX2 and Cx46 compared to GSCs as we expected (Figure 1), and the reverse in OB1-SF cell line was also observed (Figure 2). Precisely, SOX2, an essential transcription factor for the maintenance of embryonic stem cells, was overexpressed in GSCs of GBM02-SF and OB1-SF, as we expected.

Our results from the xenotransplant emphasized that the tumor microenvironment plays a critical role in the GBM differentiation status because we saw a tumor development after GBM cell implantation in brain mice. Accordingly to literature, these interactions between GSCs and their niche dictate the balance between GSCs and non-GSCs through the variation of growth factors, extracellular matrix components, and the ability to communicate with adjacent cells by gap junctions [21,22,46,47]. Among all these factors, besides the study of stem-like cell markers' expression, we assessed the profile expression of proteins involved in gap junction–mediated intercellular communication because they can sustain coordinated responses important to tumor growth, differentiation, and therapy success. Specifically, we analyzed the expression of connexins, Cx43 and Cx46, in GSCs and non-GSCs *in vitro* in order to understand their expression in the stem cell state (Figure 6).

Our results showed that, in all GBM cell lines, Cx43 protein was overexpressed in non-GSC cell lines, whereas Cx46 was upregulated

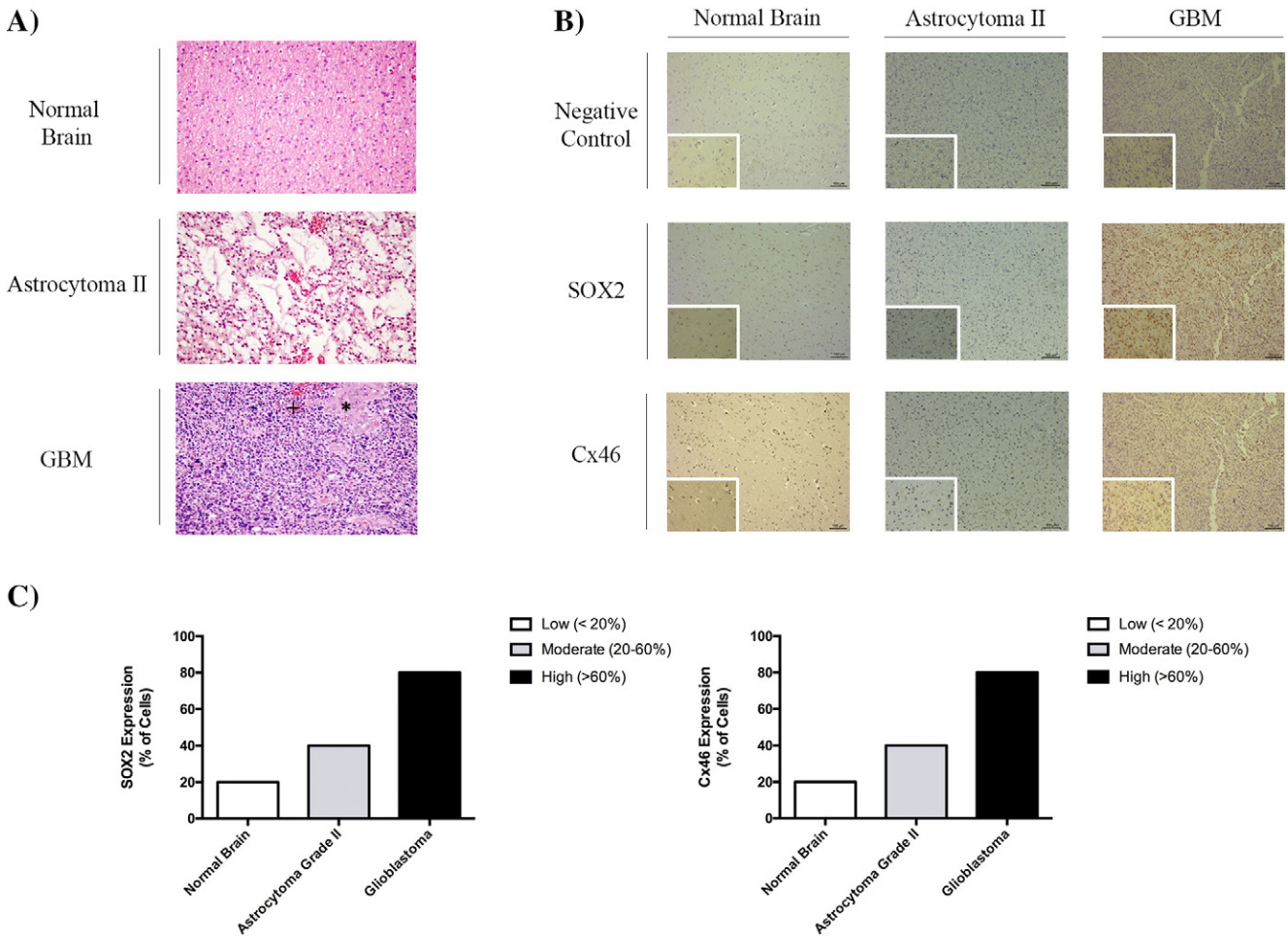

Figure 8. Analysis of SOX2 and Cx46 expression in glioblastoma, astrocytoma grade II, and normal human brain tissues by immunohistochemistry. Patients with clinical evidence of disease, MRI- and histologically confirmed diagnosis of astrocytoma grade II and astrocytoma grade IV (GBM) based on the World Health Organization (WHO) 2007 criteria [4], and who gave written informed consent to participate in the study were included. To compare the SOX2 and Cx46 expression, normal brain samples from patients that underwent an epilepsy surgery with mesial sclerosis were also analyzed. The study was approved by the University Hospital of Coimbra Ethics Committee, according to the Declaration of Helsinki protocol. (A) Histopathological characteristics of the tumor mass were evaluated by hematoxylin-eosin staining. The normal brain picture was acquired from the white matter. The astrocytoma grade II showed a nuclear atypia and microcysts, and the glioblastoma showed nuclear atypia, microvascular proliferation (+), and necrosis (*). (B) Immunohistochemistry was performed using the diaminobenzidine method with hematoxylin counterstaining to evaluate the percentage of cells expressing SOX2 and Cx46. (C) Tumor samples were ranked for SOX2 or Cx46 expression as high (60% positive cells), moderate (between 20% and 60% positive cells), and low (below 20% cells). Each image was acquired at 10× magnification (×10/0.25 PH1 NPLAN) and amplified 40× (×40/0.55 CORR PH2) (scale bar = 100 μm) with a Leica DMI3000B light microscope (Leica, Germany) and acquired with the Leica Application Suite v 4.3 (Leica, Switzerland).

in GSCs (Figure 6), which emphasizes our initial hypothesis that GSC maintenance also depends on cell-cell interactions in a connexin-isotype–dependent manner, as proposed in the study of Hitomi et al. [21].

Here, we also showed that the same cells placed in culture media with different properties sequentially alter their expression of stem-like cell markers (at times T0, T2, and T4) (Figures 1*A* and 2*A*), together with the phenotype alterations by oncospheres formation, suggesting that "stemness" is actually a state (Figures 1*B* and 2*B*). Our qPCR results endorsed these ideas (Figures 1*C* and 2*C*). The SOX2 mRNA levels were higher in stem-like conditions in both GBM02-SF cells (time T2) and OB1-SF cells (time T0). In OB1-SF cells (T4), there was a tendency of increasing SOX2 transcripts levels, but it was not statistically different. In turn, Cx43 mRNA levels were lower in stem-like statements in OB1 cells (time T0 and T4), although they were not significantly different in GBM02 cells (times T0, T2, and T4). Overall, the mRNA results are in agreement with the protein levels. To confirm this hypothesis, we tested the GSCs for the cardinal properties of stem-like cells, including their clonogenic potential, the expression of transcription factors associated with the stem state, and their ability to form tumors in an orthotopic mouse model. Examined in detail, the GBM cell lines showed differences in clonogenic potential. The GBM02-SF and GBM11-SF cell lines proved to be more capable of forming clones than the OB1-SF and U87 cell lines. These differences in the ability to form clones may be related to the intrinsic heterogeneity observed in high-grade gliomas and perhaps contribute to the different degrees of aggressiveness of GBM cells (Figure 3*B*). Interestingly, in our GSCs, the expression of

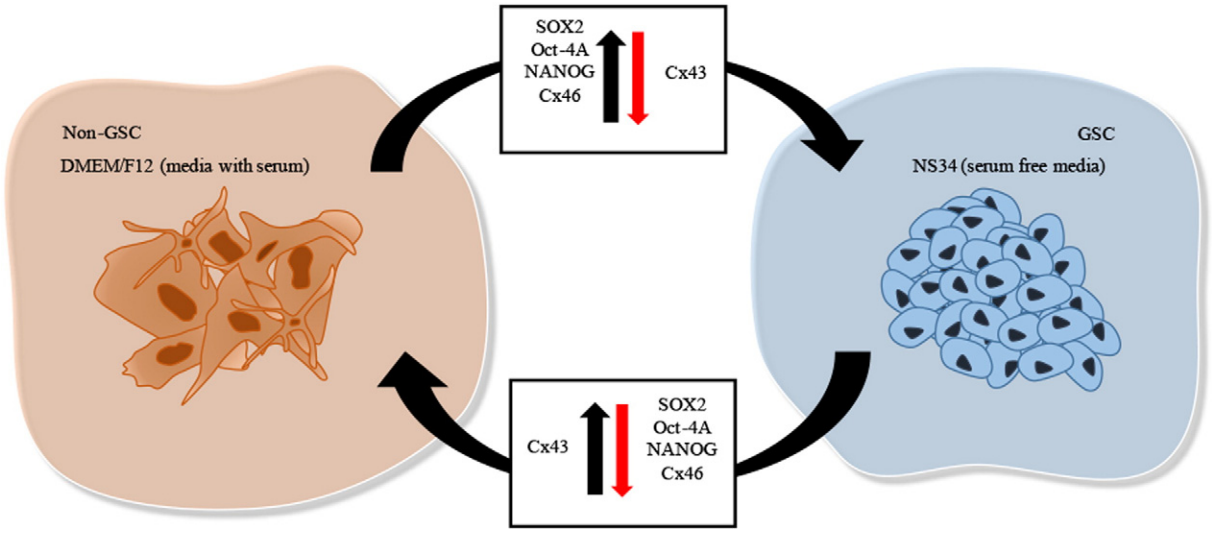

Figure 9. Plasticity of GBM stem-like cells. Interactions of GBM cells with the tumor microenvironment can dictate the dynamic balance between self-renewal and differentiation properties through growth factors present in serum-free stem-like cell medium, NS34, or through bovine-serum supplement in DMEM/F12 medium, respectively. The stem-like cell markers SOX2, OCT-4A, and Nanog differ in expression according to the stem cell state. Also, the connexins, important for cell-to-cell communication processes, demonstrate the plasticity of stem-like cells. As such, SOX2, OCT-4A, Nanog, and Cx46 are overexpressed in GSCs (green arrow), whereas Cx43 is downregulated (red arrow). In contrast, in non-GSCs, SOX2, OCT-4A, Nanog, and Cx46 are downregulated (red arrow), whereas Cx43 is overexpressed in GSCs (green arrow). Cells were imaged at 63× magnification using a DMi8 advanced fluorescence microscope (Leica Microsystems, Germany) and analyzed with Leica LA SAF Lite. Images were processed using the software ImageJ 1.49v (Wayne Rasband, National Institutes of Health).

the stem-like cell markers SOX2, Oct-4A, and NANOG was higher than in non-GSCs, as expected. These results accord with the clonogenic capability of each GBM cell line and with previous studies [23,30,48–50].

Because the stem-like properties are known to induce chemoresistance and stem cell state is dynamic, we asked if there would be a possible association between the expression of molecular markers and the aggressiveness of tumors, and their outcome (Figure 8). Therefore, we evaluated the expression of SOX2 and Cx46, both overexpressed in GSCs *in vitro*, in samples of normal, astrocytoma grade II, and astrocytoma grade IV (GBM) brains from human patients (Figure 8*A*). SOX2 and Cx46 were highly expressed in the GBM compared to the astrocytoma grade II and normal brain samples (Figure 8*B*). We classified the percentage of SOX2 and Cx46 expression in cells as low (<20% of cells expressing SOX2 or Cx46), moderate (20%-60% of cells expressing SOX2 or Cx46), and high (>60% of cells expressing SOX2 or Cx46), corresponding to the samples from normal, astrocytoma grade II, and GBM samples, respectively (Figure 8*C*). These results are in agreement with previous studies that verified a higher expression of SOX2 compared to normal brain tissue samples [20,49]. These findings suggest that GSCs are more frequent in high-grade gliomas due to unknown microenvironmental factors that could trigger the switch between stem-like and non–stem-like states in GBM. Our data reinforce the initial proposal that the stem state is a dynamic bidirectional fluctuation that depends not only but also on the microenvironment.

Summarizing, we could for the first time demonstrate the plasticity of the GBM stem-cell state, as represented in Figure 9. Briefly, the stem-like cell state is accompanied by the overexpression of markers of stem-like cells, characterized in detail by us, and by downregulation of markers of differentiated cells as expected. However, when the medium is changed, we observed that the same differentiated cells are accompanied by downregulation of stem-like cell markers and overexpression of differentiated cell markers, which showed that the stem state is not static, definitely established, but dynamic and maybe depending on tumor microenvironment.

Our results constitute an important advance in the knowledge of stem-like cells' behavior. For the first time, we showed that the GBM stem-like cell markers are dynamic and bidirectional, depending on microenvironmental clues. Because GSCs are the most chemoresistant cells in the GBM tumor mass, stem-like cell markers, such as SOX2, are more highly expressed in human GBM samples than in lower grades of gliomas, suggesting a direct correlation with the poor prognosis of GBM patients.

Altogether, our *in vitro* and *in vivo* results corroborate our hypothesis. This work highlights the understanding of GSCs and non-GSCs state, which is a primary step in comprehension of tumor growth and differentiation processes. Hopefully, these will improve the success of GBM therapy in a way to identify more specific targets to reach GBM.

Supplementary data to this article can be found online at http://dx.doi.org/10.1016/j.tranon.2017.04.005.

Conflicts of Interest

We have no conflicts of interest to declare.

Acknowledgments

We are grateful to Dr. Hervé Chneiweiss for providing the OB1 cell line. We are also grateful to Tania Spohr for providing the SOX2 Syber green primer for qPCR. This study was supported by the Brazilian agencies Conselho Nacional de Desenvolvimento Científico e Tecnológico (CNPq), Coordenação de Aperfeiçoamento de

Pessoal de Nível Superior (CAPES), Fundação de Amparo à Pesquisa do Rio de Janeiro (FAPERJ), Pró-Saúde Associação Beneficente de Assistência Social e Hospitalar, and Ary Frauzino Foundation for Cancer Research. Also, this study was also supported by FEDER funds through the Operational Programme Factors Competitiveness-COMPETE and National Funds through the FCT-Foundation for Science and Technology within the project "National funds from FCT–Fundação para a Ciência e Tecnologia" under a Ph.D. fellowship to Joana Balça Pinheiro da Costa e Silva (SFRH/BD/51993/2012) and by the project PEst-C/SAU/LA0001/2013-2014. Additional funding was granted by FEDER/COMPETE/FCT PTDC/EBB-EBI/120634/2010 and PDTC/QUI-BIQ/120652/2010 and by QREN: CENTRO-01-0762-FEDER-00204.

References

[1] Louis DN, Perry A, Reifenberger G, von Deimling A, Figarella-Branger D, Cavenee WK, Ohgaki H, Wiestler OD, Kleihues P, and Ellison DW (2016). The 2016 World Health Organization classification of tumors of the central nervous system: a summary. *Acta Neuropathol* , 1–18. http://dx.doi.org/10.1007/s00401-016-1545-1.

[2] Singh SK, Hawkins C, Clarke ID, Squire JA, Bayani J, Hide T, Henkelman RM, Cusimano MD, and Dirks PB (2004). Identification of human brain tumour initiating cells. *Nature* **432**, 396–401. http://dx.doi.org/10.1038/nature03128.

[3] Oliveira-Nunes MC, Assad Kahn S, de Oliveira Barbeitas AL, Spohr TCL de SE, Dubois LGF, Ventura Matioszek GM, Querido W, Campanati L, de Brito Neto JM, and Lima FRS, et al (2016). The availability of the embryonic TGF-β protein Nodal is dynamically regulated during glioblastoma multiforme tumorigenesis. *Cancer Cell Int* **16**, 46. http://dx.doi.org/10.1186/s12935-016-0324-3.

[4] Stupp R, Mason WP, van den Bent MJ, Weller M, Fisher B, Taphoorn MJB, Belanger K, Brandes AA, Marosi C, and Bogdahn U, et al (2005). Radiotherapy plus concomitant and adjuvant temozolomide for glioblastoma. *N Engl J Med* **352**, 987–996. http://dx.doi.org/10.1056/NEJMoa043330.

[5] Deheeger M, Lesniak MS, and Ahmed AU (2014). Cellular plasticity regulated cancer stem cell niche: a possible new mechanism of chemoresistance. *Cancer Cell Microenviron* **1**. http://dx.doi.org/10.14800/ccm.295.

[6] Huse JT, Holland E, and DeAngelis LM (2013). Glioblastoma: molecular analysis and clinical implications. *Annu Rev Med* **64**, 59–70. http://dx.doi.org/10.1146/annurev-med-100711-143028.

[7] Grossman SA, Ye X, Piantadosi S, Desideri S, Nabors LB, Rosenfeld M, Fisher J, and NABTT CNS Consortium (2010). Survival of patients with newly diagnosed glioblastoma treated with radiation and temozolomide in research studies in the United States. *Clin Cancer Res* **16**, 2443–2449. http://dx.doi.org/10.1158/1078–0432.CCR-09-3106.

[8] Singh SK, Hawkins C, Clarke ID, Squire JA, Bayani J, Hide T, Henkelman RM, Cusimano MD, and Dirks PB (2004). Identification of human brain tumour initiating cells. *Nature* **432**, 396–401. http://dx.doi.org/10.1038/nature03031.1.

[9] Ding L, Ley TJ, Larson DE, Miller CA, Koboldt DC, Welch JS, Ritchey JK, Young MA, Lamprecht T, and McLellan MD, et al (2012). Clonal evolution in relapsed acute myeloid leukaemia revealed by whole-genome sequencing. *Nature* **481**, 506–510. http://dx.doi.org/10.1038/nature10738.

[10] Schuh A, Becq J, Humphray S, Alexa A, Burns A, Clifford R, Feller SM, Grocock R, Henderson S, and Khrebtukova I, et al (2012). Monitoring chronic lymphocytic leukemia progression by whole genome sequencing reveals heterogeneous clonal evolution patterns. *Blood* **120**, 4191–4196. http://dx.doi.org/10.1182/blood-2012-05-433540.

[11] Shah SP, Roth A, Goya R, Oloumi A, Ha G, Zhao Y, Turashvili G, Ding J, Tse K, and Haffari G, et al (2012). The clonal and mutational evolution spectrum of primary triple-negative breast cancers. *Nature* **486**, 395–399. http://dx.doi.org/10.1038/nature10933.

[12] Nik-Zainal S, Van Loo P, Wedge DC, Alexandrov LB, Greenman CD, Lau KW, Raine K, Jones D, Marshall J, and Ramakrishna M, et al (2012). The life history of 21 breast cancers. *Cell* **149**, 994–1007. http://dx.doi.org/10.1016/j.cell.2012.04.023.

[13] Garcia C, Dubois L, Xavier A, Geraldo L, da Fonseca AC, Correia A, Meirelles F, Ventura G, Romão L, and Canedo NH, et al (2014). The orthotopic xenotransplant of human glioblastoma successfully recapitulates glioblastoma-microenvironment interactions in a non-immunosuppressed mouse model. *BMC Cancer* **14**, 923. http://dx.doi.org/10.1186/1471-2407-14-923.

[14] Seymour T, Nowak A, and Kakulas F (2015). Targeting aggressive cancer stem cells in glioblastoma. *Front Oncol* **5**, 159. http://dx.doi.org/10.3389/fonc.2015.00159.

[15] Todorova MG, Soria B, and Quesada I (2008). Gap junctional intercellular communication is required to maintain embryonic stem cells in a non-differentiated and proliferative state. *J Cell Physiol* **214**, 354–362. http://dx.doi.org/10.1002/jcp.21203.

[16] Naus CC and Laird DW (2010). Implications and challenges of connexin connections to cancer. *Nat Rev Cancer* **10**, 435–441. http://dx.doi.org/10.1038/nrc2841.

[17] Evans WH and Martin PEM (2002). Gap junctions: structure and function. *Mol Membr Biol* **19**, 121–136. http://dx.doi.org/10.1080/09687680210139839 [Review].

[18] Saez JC, Berthoud VM, Branes MC, Martinez AD, and Beyer EC (2003). Plasma membrane channels formed by connexins: their regulation and functions. *Physiol Rev* **83**, 1359–1400. http://dx.doi.org/10.1152/physrev.00007.2003.

[19] Orellana JA, von Bernhardi R, Giaume C, and Sáez JC (2012). Glial hemichannels and their involvement in aging and neurodegenerative diseases. *Rev Neurosci* **23**, 163–177. http://dx.doi.org/10.1515/revneuro-2011-0065.

[20] Soares AR, Martins-Marques T, Ribeiro-Rodrigues T, Ferreira JV, Catarino S, Pinho MJ, Zuzarte M, Isabel Anjo S, Manadas B, and Sluijter JPG, et al (2015). Gap junctional protein Cx43 is involved in the communication between extracellular vesicles and mammalian cells. *Sci Rep* **5**, 13243. http://dx.doi.org/10.1038/srep13243.

[21] Hitomi M, Deleyrolle LP, Mulkearns-Hubert EE, Jarrar A, Li M, Sinyuk M, Otvos B, Brunet S, Flavahan WA, and Hubert CG, et al (2015). Differential connexin function enhances self-renewal in glioblastoma. *Cell Rep* **11**, 1031–1042. http://dx.doi.org/10.1016/j.celrep.2015.04.021.

[22] Liu Y and Lu W (2012). Recent advances in brain tumor-targeted nano-drug delivery systems. *Expert Opin Drug Deliv* **9**, 671–686. http://dx.doi.org/10.1517/17425247.2012.682726.

[23] Safa AR, Saadatzadeh MR, Cohen-Gadol AA, Pollok KE, and Bijangi-Vishehsaraei K (2015). Glioblastoma stem cells (GSCs) epigenetic plasticity and interconversion between differentiated non-GSCs and GSCs. *Genes Dis* **2**, 152–163. http://dx.doi.org/10.1016/j.gendis.2015.02.001.

[24] Tata PR, Mou H, Pardo-Saganta A, Zhao R, Prabhu M, Law BM, Vinarsky V, Cho JL, Breton S, and Sahay A, et al (2013). Dedifferentiation of committed epithelial cells into stem cells in vivo. *Nature* **503**, 218–223. http://dx.doi.org/10.1038/nature12777.

[25] Chaffer CL, Brueckmann I, Scheel C, Kaestli AJ, Wiggins PA, Rodrigues LO, Brooks M, Reinhardt F, Su Y, and Polyak K, et al (2011). Normal and neoplastic nonstem cells can spontaneously convert to a stem-like state. *Proc Natl Acad Sci U S A* **108**, 7950–7955. http://dx.doi.org/10.1073/pnas.1102454108.

[26] Meacham CE and Morrison SJ (2013). Tumour heterogeneity and cancer cell plasticity. *Nature* **501**, 328–337. http://dx.doi.org/10.1038/nature12624.

[27] Easwaran H, Tsai H-C, and Baylin SB (2014). Cancer epigenetics: tumor heterogeneity, plasticity of stem-like states, and drug resistance. *Mol Cell* **54**, 716–727. http://dx.doi.org/10.1016/j.molcel.2014.05.015.

[28] Kahn SA, Biasoli D, Garcia C, Geraldo LH, Pontes B, Sobrinho M, Frauches AC, Romao L, Soletti RC, and Assuncao Fdos S, et al (2012). Equinatoxin II potentiates temozolomide- and etoposide-induced glioblastoma cell death. *Curr Top Med Chem* **12**, 2082–2093 http://www.ncbi.nlm.nih.gov/pubmed/23167797.

[29] Faria J, Romão L, Martins S, Alves T, Mendes FA, De Faria GP, Hollanda R, Takiya C, Chimelli L, and Morandi V, et al (2006). Interactive properties of human glioblastoma cells with brain neurons in culture and neuronal modulation of glial laminin organization. *Differentiation* **74**, 562–572. http://dx.doi.org/10.1111/j.1432–0436.2006.00090.x.

[30] Patru C, Romao L, Varlet P, Coulombel L, Raponi E, Cadusseau J, Renault-Mihara F, Thirant C, Leonard N, and Berhneim A, et al (2010). CD133, CD15/SSEA-1, CD34 or side populations do not resume tumor-initiating properties of long-term cultured cancer stem cells from human malignant glio-neuronal tumors. *BMC Cancer* **10**, 66. http://dx.doi.org/10.1186/1471-2407-10-66.

[31] Thirant C, Bessette B, Varlet P, Puget S, Cadusseau J, Tavares SDR, Studler J-M, Silvestre DC, Susini A, and Villa C, et al (2011). Clinical relevance of tumor cells with stem-like properties in pediatric brain tumors. *PLoS One* **6**, e16375. http://dx.doi.org/10.1371/journal.pone.0016375.

[32] Towbin H, Staehelin T, and Gordon J (1989). Immunoblotting in the clinical laboratory. *J Clin Chem Clin Biochem* **27**, 495–501 [http://www.ncbi.nlm.nih.gov/pubmed/2681521 accessed October 18, 2016].

[33] Balça-Silva J, Matias D, Do Carmo A, Girão H, Moura-Neto V, Sarmento-Ribeiro AB, and Lopes MC (2015). Tamoxifen in combination with temozolomide induce a synergistic inhibition of PKC-pan in GBM cell lines. *Biochim Biophys Acta* **1850**, 722–732. http://dx.doi.org/10.1016/j.bbagen.2014.12.022.

[34] Pfaffl MW (2001). A new mathematical model for relative quantification in real-time RT-PCR. *Nucleic Acids Res* **29**, e45 [http://www.ncbi.nlm.nih.gov/pubmed/11328886 accessed April 14, 2017].

[35] Reference JE (1985). Bottenstein, product info_N2-K; 1985.

[36] Brewer GJ (1995). Serum-free B27/neurobasal medium supports differentiated growth of neurons from the striatum, substantia nigra, septum, cerebral cortex, cerebellum, and dentate gyrus. *J Neurosci Res* **42**, 674–683. http://dx.doi.org/10.1002/jnr.490420510.

[37] Tam WL and Weinberg RA (2013). The epigenetics of epithelial-mesenchymal plasticity in cancer. *Nat Med* **19**, 1438–1449. http://dx.doi.org/10.1038/nm.3336.

[38] Tania M, Khan MA, and Fu J (2014). Epithelial to mesenchymal transition inducing transcription factors and metastatic cancer. *Tumour Biol* **35**, 7335–7342. http://dx.doi.org/10.1007/s13277-014-2163-y.

[39] Mallini P, Lennard T, Kirby J, and Meeson A (2014). Epithelial-to-mesenchymal transition: what is the impact on breast cancer stem cells and drug resistance. *Cancer Treat Rev* **40**, 341–348. http://dx.doi.org/10.1016/j.ctrv.2013.09.008.

[40] Soroceanu L, Manning TJ, and Sontheimer H (2001). Reduced expression of connexin-43 and functional gap junction coupling in human gliomas. *Glia* **33**, 107–117 [http://www.ncbi.nlm.nih.gov/pubmed/11180508 accessed October 18, 2016].

[41] Lima FRS, Kahn SA, Soletti RC, Biasoli D, Alves T, da Fonseca ACC, Garcia C, Romão L, Brito J, and Holanda-Afonso R, et al (2012). Glioblastoma: therapeutic challenges, what lies ahead. *Biochim Biophys Acta* **1826**, 338–349. http://dx.doi.org/10.1016/j.bbcan.2012.05.004.

[42] Dubois LG, Campanati L, Righy C, D'Andrea-Meira I, Spohr TCL de SE, Porto-Carreiro I, Pereira CM, Balça-Silva J, Kahn SA, and DosSantos MF, et al (2014). Gliomas and the vascular fragility of the blood brain barrier. *Front Cell Neurosci* **8**, 418. http://dx.doi.org/10.3389/fncel.2014.00418.

[43] Stupp R, Hegi ME, Mason WP, van den Bent MJ, Taphoorn MJB, Janzer RC, Ludwin SK, Allgeier A, Fisher B, and Belanger K, et al (2009). Effects of radiotherapy with concomitant and adjuvant temozolomide versus radiotherapy alone on survival in glioblastoma in a randomised phase III study: 5-year analysis of the EORTC-NCIC trial. *Lancet Oncol* **10**, 459–466. http://dx.doi.org/10.1016/S1470–2045(09)70025-7.

[44] Diaz A and Leon K (2011). Therapeutic approaches to target cancer stem cells. *Cancers (Basel)* **3**, 3331–3352. http://dx.doi.org/10.3390/cancers3033331.

[45] Ortensi B, Setti M, Osti D, and Pelicci G (2013). Cancer stem cell contribution to glioblastoma invasiveness. *Stem Cell Res Ther* **4**, 18. http://dx.doi.org/10.1186/scrt166.

[46] Visvader JE and Lindeman GJ (2012). Cancer stem cells: current status and evolving complexities. *Cell Stem Cell* **10**, 717–728. http://dx.doi.org/10.1016/j.stem.2012.05.007.

[47] Wei C-J, Xu X, and Lo CW (2004). Connexins and cell signaling in development and disease. *Annu Rev Cell Dev Biol* **20**, 811–838. http://dx.doi.org/10.1146/annurev.cellbio.19.111301.144309.

[48] Würth R, Barbieri F, and Florio T (2014). New molecules and old drugs as emerging approaches to selectively target human glioblastoma cancer stem cells. *Biomed Res Int* **2014**, 126586. http://dx.doi.org/10.1155/2014/126586.

[49] Jackson M, Hassiotou F, and Nowak A (2015). Glioblastoma stem-like cells: at the root of tumor recurrence and a therapeutic target. *Carcinogenesis* **36**, 177–185. http://dx.doi.org/10.1093/carcin/bgu243.

[50] Altaner C and Altanerova V (2012). Stem cell based glioblastoma gene therapy. *Neoplasma* **59**, 756–760. http://dx.doi.org/10.4149/neo_2012_95.